Large eddy simulation of flame edge evolution in a spark-ignited methane-air jet

(Accepted for publication in Proc. Combust. Inst., 02/06/2016)

Z. Chen*, S. Ruan, N. Swaminathan

Department of Engineering, University of Cambridge, Cambridge CB2 1PZ, UK

Abstract

The unsteady evolution of lifted methane-air jet flames following spark ignition is computed using Large Eddy Simulation (LES). A presumed joint Probability Density Function (PDF) approach is used for the sub-grid combustion modelling accounting for both premixed and non-premixed mode contributions. Two flames, one with high and another with low jet velocities are investigated and the computed temporal variation of flame leading point agrees quite well with the measured data for both the transient evolution and final lift-off height. The joint PDF of the axial and radial stabilisation locations shows that these locations are correlated with the jet exit velocity. The flame leading point evolution in the three-dimensional physical space is visualised using its trajectory, starting from the ignition location to the final lift-off height. A *spiral*-shaped path is observed for both velocity cases showing different flame propagation behaviours at different heights from the jet exit. These observations are explained on a physical basis.

Keywords: Large Eddy Simulation; Spark ignition; Flame propagation; Lift-off

*Corresponding author.
Email address: zc252@cam.ac.uk (Z. Chen)

height; Partially premixed combustion

1. Introduction

Spark ignition (or *forced ignition*) process involving a transient growth of an initial flame kernel to a fully burning flame is crucial for many practical devices [1]. In non-premixed combustion systems, an edge flame usually forms following a successful kernel initiation and its subsequent propagation in compositionally inhomogeneous mixtures experiences strong turbulence/chemistry interaction [2–4]. Therefore, understanding the underlying physics of this transient process is of prime importance to develop practical control strategies especially for high-altitude operating aero gas turbines and rocket engines.

Many experimental and numerical works investigated spark ignition and the following flame propagation in various non-premixed systems (see [1] for a review). Among these efforts, the lifted jet flame is widely considered because of its simple geometry and rich physics involving partial premixing, edge flame propagation and triple flames [5–7]. Following the works of Birch et al. [8, 9], Ahmed and Mastorakos [10] investigated ignition probability and lift-off evolution in a methane-air jet with a range of flow and composition conditions. The temporal evolution of flame leading point from ignition to stabilisation was measured using high-speed movie for two jet velocities and a flame propagation speed was estimated using the mean flow velocity deduced from a correlation [11]. However, there is a considerable room for error due to the crude estimations used as suggested in [10]. Therefore, modelling efforts are required to shed insight on edge flame propagation and its interaction with flow field. Müller et al. [12] computed a propagating jet flame using two-dimensional unsteady Reynolds-averaged

Navier-Stokes (2D-URANS) method with a G-equation fomulation for partially premixed flame and found that the physical processes had varying effects at different heights from the jet exit. Chen et al. [13] showed a substantial difference between the measured [10] flame leading point evolution and that computed using flamelets, and noted that advanced method was required to capture the transient evolution.

Large Eddy Simulation (LES) is well suited for this and becoming attractive because of rapid advances in computing and sub-grid scale (SGS) model development. LES resolves energy containing large scales and thus one can examine the interaction between edge flame and large-scale flow structures. Numerous LES with various SGS combustion models were conducted to study fully burning turbulent flames, see reviews in [14, 15] and flames in practical applications [16–18]. These studies are not reviewed here because the current focus is on the transient evolution of lifted flames. Lacaze et al. [19] computed a high-velocity (25.5 m/s) jet flame in [10] using thickened flame model and found a quite good agreement with the measurements of both the final lift-off height and transient evolution of flame leading point. This evolution was studied by comparing LES snapshots and line-of-sight experimental images. Jones and Prasad [20] calculated the low-velocity (12.5 m/s) flame in [10] using a filtered Probability Density Function (PDF) approach with Eulerian stochastic fields. A good agreement with the measurements was observed.

The objective of this paper is to investigate the lifted flame propagation and its interaction with the turbulent flow using LES with a presumed joint sub-grid PDF approach for partially premixed combustion. The flame leading edge evolution in azimuthal direction is of particular interest because the propagation is sensitive

to the local flow and stoichiometry. Also, this specific point is not addressed in previous studies. Hence lifted flames for both jet velocities (12.5 and 25.5 m/s) are computed to examine the influence of flow and mixing conditions on its transient evolution.

The paper is organised as follows. The combustion model is decribed in Section 2, followed by the experimental and numerical details in Section 3. The results are discussed in Section 4 and finally the conclusions are summarised in Section 5.

2. Modelling methodology

2.1. LES governing equations

The Favre-filtered conservation equations for mass, momentum and total enthalpy are solved. The unresolved sub-grid stress tensor, $\boldsymbol{\tau}_{\text{sgs}} \equiv \overline{\rho}(\widetilde{\boldsymbol{u}\boldsymbol{u}} - \widetilde{\boldsymbol{u}}\,\widetilde{\boldsymbol{u}})$, is closed using the Smagorinsky model [21]: $\mu_{\text{sgs}} = \overline{\rho}\,(C_S\Delta)^2\|\widetilde{\boldsymbol{S}}\|$, where $C_S = 0.167$, $\|\widetilde{\boldsymbol{S}}\|$ is the filtered rate of strain [22] and $\overline{\rho}$ is the filtered density. The filter width Δ is computed as the cube root of the local numerical cell volume.

As chemical reactions are SGS phenomena, they require modelling and a flamelet-based partially premixed combustion model is proposed based on the framework in [13, 23]. This LES model maps all thermo-chemical quantities into a low-dimensional manifold characterised by mixture fraction, Z, and a reaction progress variable, c, and utilises a presumed joint sub-grid PDF for Z and c. The mixture fraction is defined using Bilger's formula [24] and $c = \psi \,/\, \psi^{\text{Eq}}$ is used, where $\psi = Y_{\text{CO}} + Y_{\text{CO}_2}$ and ψ^{Eq} is its equilibrium value for the local mixture [13, 23]. The filtered values and sub-grid variances of Z and c are computed in LES using their transport equations. These Favre-filtered transport equations, in

standard notations, are

$$\overline{\rho}\,\widetilde{\mathscr{D}}_t\widetilde{Z} = \nabla\cdot\left(\overline{\rho}\widetilde{D}\nabla\widetilde{Z} - \overline{\rho}\widetilde{\boldsymbol{u}''Z''}\right), \tag{1}$$

$$\begin{aligned}\overline{\rho}\,\widetilde{\mathscr{D}}_t\widetilde{Z''^2} &= \nabla\cdot\left(\overline{\rho}\widetilde{D}\nabla\widetilde{Z''^2} - \overline{\rho}\widetilde{\boldsymbol{u}''Z''^2}\right)\\ &\quad - 2\overline{\rho}\widetilde{\chi}_{Z,\mathrm{sgs}} - 2\overline{\rho}\widetilde{\boldsymbol{u}''Z''}\cdot\nabla\widetilde{Z},\end{aligned} \tag{2}$$

$$\overline{\rho}\,\widetilde{\mathscr{D}}_t\widetilde{c} = \nabla\cdot\left(\overline{\rho}\widetilde{D}\nabla\widetilde{c} - \overline{\rho}\widetilde{\boldsymbol{u}''c''}\right) + \overline{\dot{\omega}_c^*}, \tag{3}$$

and

$$\begin{aligned}\overline{\rho}\,\widetilde{\mathscr{D}}_t\widetilde{c''^2} &= \nabla\cdot\left(\overline{\rho}\widetilde{D}\nabla\widetilde{c''^2} - \overline{\rho}\widetilde{\boldsymbol{u}''c''^2}\right) - 2\overline{\rho}\widetilde{\chi}_{c,\mathrm{sgs}}\\ &\quad - 2\overline{\rho}\widetilde{\boldsymbol{u}''c''}\cdot\nabla\widetilde{c} + 2(\overline{c\,\dot{\omega}_c^*} - \widetilde{c}\,\overline{\dot{\omega}_c^*}),\end{aligned} \tag{4}$$

where $\widetilde{\mathscr{D}}_t \equiv (\partial_t + \widetilde{\boldsymbol{u}}\cdot\nabla)$ is the substantial derivative and $\widetilde{D}$ is the molecular diffusivity. The sub-grid fluxes are modelled using the gradient transport approximation, for example, $\overline{\rho}\widetilde{\boldsymbol{u}''Z''} = -\overline{\rho}\nu_t\nabla\widetilde{Z}/\mathrm{Sc}_t$, where $\mathrm{Sc}_t = 0.4$ [25] and ν_t is the SGS eddy viscosity. The SGS scalar dissipation rate of mixture fraction is modelled as $\widetilde{\chi}_{Z,\mathrm{sgs}} = C_Z(\nu_t/\Delta^2)\widetilde{Z''^2}$, with the commonly used coefficient $C_Z = 2$ [14]. For the progress variable dissipation rate, models purely based on mixing timescale are inadequate [26] and thus the algebraic model proposed in [27] for premixed combustion is modified to include the effects of mixture stratification and this model is

$$\begin{aligned}\widetilde{\chi}_{c,\mathrm{sgs}} &= \mathscr{F}_0\Big[2K_c^*(S_L^0/\delta_L^0)\\ &\quad + (C_3 - \tau C_4\mathrm{Da}_\Delta)(2u'_\Delta/3\Delta)\Big]\widetilde{c''^2}/\beta_c',\end{aligned} \tag{5}$$

where $u'_\Delta = |\widehat{\widetilde{\boldsymbol{u}}} - \widetilde{\boldsymbol{u}}|$ is the SGS velocity obtained using a test filter width of $\widehat{\Delta} = 2\Delta$. The function $\mathscr{F}_0 = \left(1 - e^{-0.75\Delta/\delta_L^0}\right)$ ensures that $\widetilde{\chi}_{c,\mathrm{sgs}}$ approaches 0

when Δ/δ_L^0 is small. Da_Δ is the SGS Damköhler number and, C_3, C_4 and $\beta_c^{'}$ are model parameters as detailed in [27, 28]. C_3 and C_4 do not have any tunable parameters and are calculated on the fly using local flow and flame attributes. $\beta_c^{'}$ value can be determined through a dynamic procedure [28] but it is taken to be 7.5 for simplicity here. The other parameters in Eq. (5), K_c^*, τ, S_{L}^0 and δ_{L}^0, vary with the local equivalence ratio, and these values are obtained from unstrained planar laminar flame calculations. The reaction source terms $\overline{\dot{\omega}_c^*}$ and $\overline{c\,\dot{\omega}_c^*}$ in Eqs. (3) and (4) are modelled as described next.

2.2. LES sub-grid combustion model

As the combustion is partially premixed in the stabilisation region of lifted flames [3, 4], a sub-grid model accounting for both premixed and non-premixed combustion is required. Following [13] and [23], the reaction rate in Eq. (3) is written as

$$\overline{\dot{\omega}_c^*} = \overline{\dot{\omega}}_c + \overline{\dot{\omega}}_{\mathrm{np}} = \overline{\dot{\omega}}_c + \overline{\rho N_{ZZ} \frac{c}{\psi^{\mathrm{Eq}}} \frac{d^2\psi^{\mathrm{Eq}}}{dZ^2}}\ , \tag{6}$$

where $N_{ZZ} \equiv D(\nabla Z \cdot \nabla Z)$ is the instantaneous dissipation rate of mixture fraction. The $\overline{\dot{\omega}}_c$ and $\overline{\dot{\omega}}_{\mathrm{np}}$ signify the contributions from premixed and non-premixed combustion respectively.

In this study, $\overline{\dot{\omega}}_c$ is modelled as

$$\overline{\dot{\omega}}_c = \int_0^1 \int_0^1 \dot{\omega}_c(\xi,\zeta)\ P_\Delta(\xi,\zeta)\quad d\xi\ d\zeta\ , \tag{7}$$

where ξ and ζ are the sample space variables for Z and c respectively. The flamelet reaction rate $\dot{\omega}_c(\xi,\zeta)$ is obtained from laminar flame calculations. To account for the SGS fluctuations of both Z and c, the SGS joint PDF, $P_\Delta(\xi,\zeta)$, is modelled as $P_\Delta(\xi,\zeta) = P_\Delta(\xi;\widetilde{Z},\widetilde{Z''^2})P_\Delta(\zeta;\widetilde{c},\widetilde{c''^2})$ using two Beta PDFs.

The non-premixed contribution in Eq. (6) is modelled as

$$\overline{\dot{\omega}}_{\rm np} \simeq \overline{\rho}\,\widetilde{c}\widetilde{\chi}_Z \int_0^1 \frac{1}{\psi^{\rm Eq}(\xi)} \frac{d^2\psi^{\rm Eq}(\xi)}{d\xi^2}\, \widetilde{P}_\Delta(\xi)\, d\xi, \tag{8}$$

to include the SGS effects of mixture fraction fluctuation. The filtered scalar dissipation rate is the sum of resolved and SGS parts, $\widetilde{\chi}_Z = \widetilde{D}(\nabla\widetilde{Z}\cdot\nabla\widetilde{Z}) + \widetilde{\chi}_{Z,\,\rm sgs}$. The reaction related term $\overline{c\,\dot{\omega}_c^*}$ in Eq. (4) is modelled in a manner consistent with Eq. (7). The filtered temperature, $\widetilde{T}$, is obtained using the transported total enthalpy, $\widetilde{h}$, as detailed in [28] and this temperature is used to calculate the filtered density through the equation of state.

3. Experimental configuration and numerical setup

The experiments of Ahmed and Mastorakos [10] investigating lifted flames of air-diluted (30% air by volume) methane jet issuing into ambient air at two bulk mean velocities of $\upsilon_{\rm j}$ = 12.5 and 25.5 m/s are considered. The jet diameter, $d_{\rm j}$, was 5 mm and a co-axial airflow at 0.1 m/s was introduced through an annulus having outer diameter of 200 mm to avoid ambient disturbances. The spark was placed at different locations and no substantial difference was observed for the transient flame evolution and final lift-off height. The axial position of flame leading point was measured using high-speed movies and 10 experiments were conducted for each jet velocity to get ensemble-averaged results. A scatter of 9% was reported for the measurements of flame leading edge position.

The cylindrical LES computational domain spans from the jet exit plane to $200d_{\rm j}\times100d_{\rm j}\times2\pi$ in the axial (z), radial (r) and azimuthal (θ) directions respectively. An unstructured grid with 7M tetrahedra cells is used with the smallest filter width of Δ = 0.3 mm located in the near-nozzle region. Refined mesh is

Table 1. Summary of computed flame details.

Flame	Air	v_j (m/s)	Re	Ignition
F1	30%	12.5	3759	30 d_j
F2	30%	25.5	7669	30 d_j

also applied in the shear layer to resolve the majority of turbulent kinetic energy. The mean axial jet velocity is specified using a 1/7th power law and a 5% random noise is given for the velocity fluctuation. The comprehensive chemical mechanism GRI-Mech 3.0 is used for this study and the quenching mixture fraction dissipation rate at stoichiometry given by this mechanism is, $(\chi_{Z,q})_{st} = 5\ s^{-1}$, which is consistent with previous studies [4, 12]. The CFD toolbox OpenFOAM is used and the built-in thermo-physical model for the LES solver is replaced by the combustion model described in Section 2. Second-order numerical schemes are used for both temporal and spatial discretisations. A relatively small time-step size of 0.4 μs is used so that the CFL number is below 0.3 in the entire computational domain. The computation is performed using 1080 cores on the ARCHER UK National Supercomputer and a typical ignition sequence of 600 ms in physical time requires about 60 hours of wall-clock time.

The two cases considered here are listed in Table 1. The same ignition location of $30d_j$ on the centreline is used to investigate the influence of flow structures on the transient flame propagation. Fully developed cold mixing flow is obtained before igniting the flame. The numerical ignition is initiated by specifying $\widetilde{c} = 1$ in a spherical sub-domain with a diameter of 2 mm, which provides an equivalent energy deposition of about 100 mJ as in the experiments [10].

4. Results and discussion

4.1. Cold flow

The axial velocity statistics of an air jet with a bulk mean velocity of $\upsilon_j = 21$ m/s are shown in Fig. 1. The computed centreline variation of the normalised mean axial velocity agrees well with the correlation of Tieszen et al. [11] as in Fig. 1a. υ_{cl} is the centreline velocity and υ_c is the co-flow air velocity. About 5% difference is observed, which is similar to those in earlier studies [19, 20] and is possibly due to same small difference in the turbulence given at the jet inlet boundary. Unfortunately, this turbulence was not characterised in the experiments. Figures 1b and 1c compare the radial variations of computed and measured [10] normalised mean axial velocity and its rms values for four axial locations. A good agreement is seen for the mean velocity, and the rms values are over-predicted by about 5-10%. In general, the cold flow characteristics are captured reasonably well by the LES.

4.2. Flame edge transient evolution

Ahmed and Mastorakos [10] observed four typical flame evolution stages in their experiments following a successful ignition, namely the flame kernel growth, radial expansion, leading edge upstream propagation and final stabilisation stage at the lift-off height. Qualitative comparison between the experimental instantaneous images and LES snapshots has been shown in previous studies [17, 20] and similar flame topologies are also observed in the present simulations but it is not discussed further here since the focus of this study is on the transient evolution of the flame edge. After the spherical kernel has fully grown, an edge flame forms during the radial expansion stage as in Fig. 2, showing the reaction rate

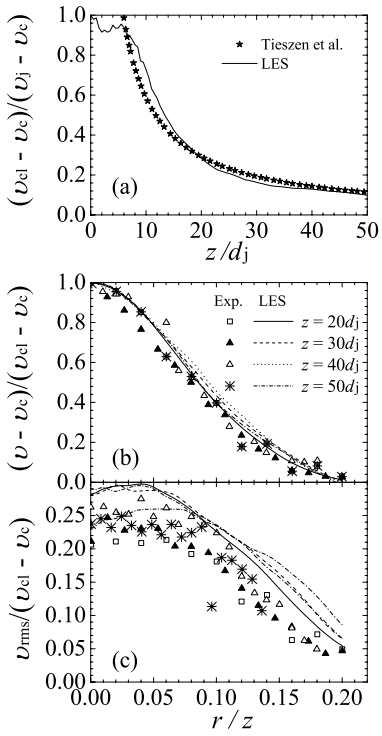

Fig. 1. Comparison of cold flow statistics of axial velocity, (a) centreline variation (b) radial variations of mean velocity (c) radial variations of rms velocity.

of progress variable along with the mixture fraction iso-lines. It is observed that the formation starts from a rich mixture on the jet centreline in Fig. 2a, and then expands radially across the stoichiometric line in Fig. 2b and finally establishes a leading edge in the relatively lean mixture as highlighted in Fig. 2c. Subsequently, this edge flame starts to propagate upstream interacting with the oncoming flow, shown by the wrinkled flame structure. During this process, the reaction rate is well contained within the flammability limits suggesting a good model prediction for the edge flame evolution.

The earlier studies [17, 20] compared the LES slices and line-of-sight exper-

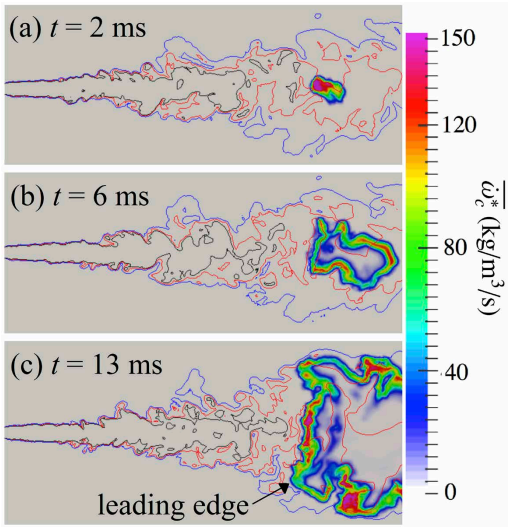

Fig. 2. Middle-plane snapshots of the reaction rate of progress variable, $\overline{\dot{\omega}_c^*}$ in flame F2. The iso-lines are stoichiometry (red), rich (black) and lean (blue) flammability limits.

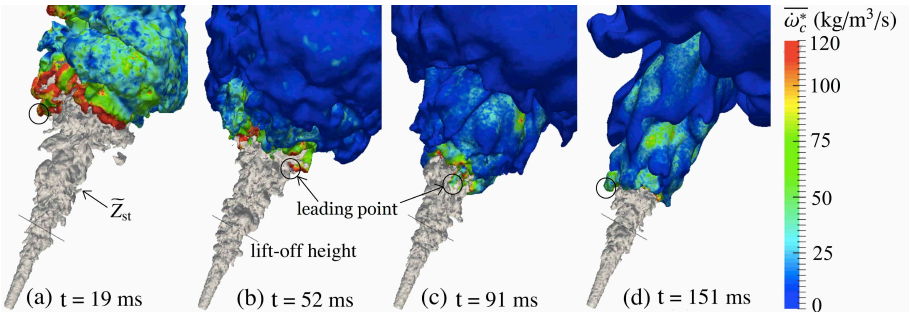

Fig. 3. Transient evolution of flame F2 leading edge marked using $\widetilde{T}$=1200 K iso-surface coloured by $\overline{\dot{\omega}_c^*}$.

imental images qualitatively to study the edge flame propagation. To investigate this process further, the flame behaviour in the 3D space needs to be considered because the flame leading edge does not reside in the same z-r plane because of its evolution in the azimuthal direction. This is illustrated in Fig. 3 showing typical

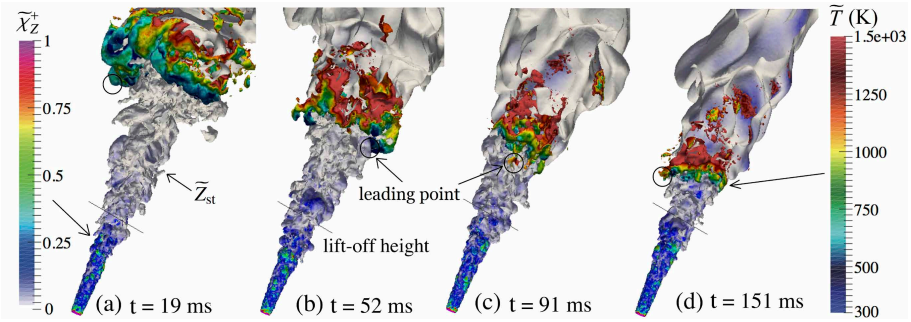

Fig. 4. Transient evolution of flame F2 leading edge marked using $\overline{\dot{\omega}_c^*}$=80 kg/m^3/s iso-surface coloured by $\widetilde{T}$ (top part). The $\widetilde{Z}_{st}$ iso-contour is coloured by a normalised scalar dissipation rate $\widetilde{\chi}_Z^+$ (bottom part).

3D evolution of the leading edge at four instants after ignition using $\widetilde{T}$ = 1200 K [13] iso-surface coloured by $\overline{\dot{\omega}_c^*}$. The iso-contour of the stoichiometric mixture fraction is also shown to visualise the flow and mixing fields. As highlighted by the black circles, the leading point appears at different azimuthal positions at different times as in Fig. 3. The local reaction rate at these points seems to vary largely, with high values over 100 kg/m^3/s for t = 19 and 52 ms and lower values of around 75 kg/m^3/s for 91 and 151 ms. To shed more light on this, Fig. 4 plots a typical iso-surface of $\overline{\dot{\omega}_c^*}$ = 80 kg/m^3/s coloured by $\widetilde{T}$ at the same instants as in Fig. 3. Similar leading point locations are observed in these two figures suggesting that the leading point marker chosen using $\widetilde{T}$ can represent the flame leading edge quite well. In Fig. 4, the $\widetilde{Z}_{st}$ iso-surface is coloured by its filtered scalar dissipation rate, which is normalised as $\widetilde{\chi}_Z^+ = \widetilde{\chi}_Z / (\chi_{Z,q})_{st}$, where $(\chi_{Z,q})_{st}$ is a reference quenching dissipation rate noted in section 3. It is shown that $\widetilde{\chi}_Z^+ << 1$ at the lift-off height and its downstream, consistent with previous studies [12, 13, 23].

Furthermore, the radial position of the leading point also varies from one instant to another because of the difference in local mixing conditions. A *finger-like*

shape at the leading point is observed in Figs. 3a and 3d and this is outside the stoichiometric surface indicating lean mixture, whereas the leading point is found close to the stoichiometry in Figs. 3b and 3c. This is because the turbulent flow generates fuel pockets far from the jet centre and these ignited pockets propagate faster than the main flame as the local velocity is relatively small. Once the fuel in the pocket has been fully consumed, these branches extinguish and the leading point moves close to the stoichiometry. These flame propagation behaviours suggest that the large-scale flame/flow interaction plays an important role in the transient evolution of the leading edge.

The axial position of the most upstream point of the leading edge was measured in [10] at various times covering the entire ignition sequence. The averaged results are obtained by ensemble averaging 10 samples for each of flames F1 and F2. These results are shown in Fig. 5 along with the computational results. A good overall agreement is observed for both flames, however, the final lift-off height of F1 is over-predicted by about $2d_{\mathrm{j}}$, which is similar to that in [20]. This is possibly due to the fast-decaying random fluctuation given at the inlet boundary yielding under-predicted turbulent mixing in the near jet exit region (about $3d_{\mathrm{j}}$) where flame F1 is stabilised. The partially premixed combustion occurs in the stabilisation region and thus the assumption of statistical independence for the sub-grid fluctuations of Z and c may not hold. The Z-c correlation was shown to be important for RANS [13, 23] but its role for SGS modelling is unclear. The difference seen in Fig. 5 for the lift-off height may also be due to this assumption. Further investigations are required. Nevertheless, the transient evolution of the flame leading point during the entire ignition sequence is captured reasonably in the LES using the partially premixed combustion model proposed here and is

similar to the prediction obtained using thickened flame [17] and LES-PDF [20] methods.

Two sub-stages of flame propagation are noted in Fig. 5. In the beginning, the thermo-chemistry is stronger than the convection at the leading edge yielding a high net propagation speed and this process is called as the freely propagating sub-stage, which is from 5 to 130 ms for F1, and from 15 to 240 ms for F2 flames. The dominant thermo-chemical effect is reflected by the large $\overline{\dot{\omega}_c^*}$ in Fig. 3a and 3b. The second sub-stage is the stabilising process; the leading point enters the stabilisation region with high turbulence but still moves upstream slowly until the final lift-off height is reached. The flame propagation behaviour during these sub-stages is further discussed later.

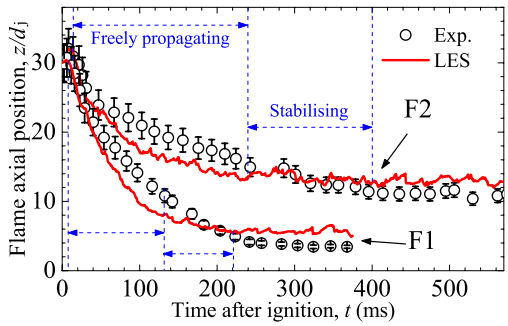

Fig. 5. Transient evolution of measured and computed flame leading point. The error bars correspond to the 9% maximum scatter of the experimental data [10].

Figure 6 presents the 3D travel path of the leading point from the ignition location to final lift-off height for both flames F1 and F2. The trajectory shown is from single LES realisation of these two flames and different spiral trajectories are expected from different realisations. The scatter plotted on the stabilisation plane show the radial and azimuthal variation of the stabilisation location at the

lift-off height. The arrows near the ignition plane demonstrate the initial downstream kernel convection and radial expansion stages, and the red arrows indicate the direction of increasing time. The leading point trajectory seems to follow a *spiral*-shaped trajectory during the evolution of both F1 and F2. The kernel is convected downstream initially almost along the jet axis which is clearer for F2 due to higher flow velocity. Different expansion directions are observed for F1 and F2 leading to different subsequent travel paths as in Figs. 6a and 6b. This is because of the difference in the local mixing conditions. However, there will be equal probability for the initial radial expansion of the flame to occur in any angle. After this expansion, the leading point moves upstream with further radial expansion until a maximum radial distance is reached. This distance seems to be independent of the jet velocity and it is about $5d_{\mathrm{j}}$ in both Figs. 6a and 6b. The flame propagation dominates during this phase, which corresponds to the freely propagating sub-stage identified earlier, and the flame/flow interaction is reflected through the mixing by directing the leading edge to the most reactive spots. These spots are controlled by the local conditions of the mixture and flow-straining dictated by large-scale motion. In the stabilising sub-stage, as the flame approaches the region close to the lift-off height below $10d_{\mathrm{j}}$ for F1 and $20d_{\mathrm{j}}$ for F2, the leading point move closer to the centreline. The large fluctuation seen there is caused by strong interaction between the leading edge and the oncoming flow with mixtures beyond the flammability limits creating local extinctions. In the final stage of stabilisation, the leading point randomly moves around the centreline. This random motion shown as scattered points projected on the final stabilisation plane suggests an approximate circular motion. This approximate circle diameter shown in Fig. 6b for flame F2 is evidently larger than that for F1 in Fig. 6a and this influence

of the jet velocity is further discussed by examining the lift-off statistics next.

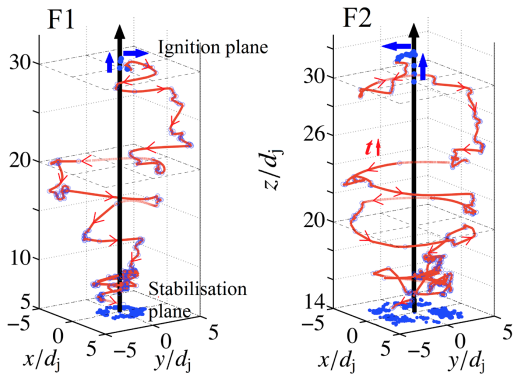

Fig. 6. 3D visualisation of the flame leading point trajectory.

4.3. Lift-off statistics

The flame stabilisation location oscillates by about one to $2d_j$ in both axial and radial directions depending on the jet exit velocity. These oscillations result from unsteadiness in the oncoming and entrained flows. The radial location moves outward as the flame leading edge moves downstream and *vice versa*. These correlated movements can be seen in Fig. 7 showing the joint PDF of the axial, L_f, and radial, R_f, locations of the stabilisation point for both F1 and F2. This PDF is constructed using 500 samples collected over 250 ms. The iso-lines shown are based on the time averaged mixture fraction field. These radial and axial coordinates are normalised using the jet diameter, d_j, or a representative length scale, $U_j\tau_L$, where $\tau = (\delta_L^0/S_L^0)_{st}$. The stabilisation point with the highest probability is observed around $L_f = 5.7d_j$ and $R_f = 1.7d_j$ for F1. In contrast, flame F2 is stabilised at $L_f = 13.2d_j$ and $R_f = 2.7d_j$, further away from the jet exit and centreline. These axial and radial locations and also their fluctuations seem to collapse

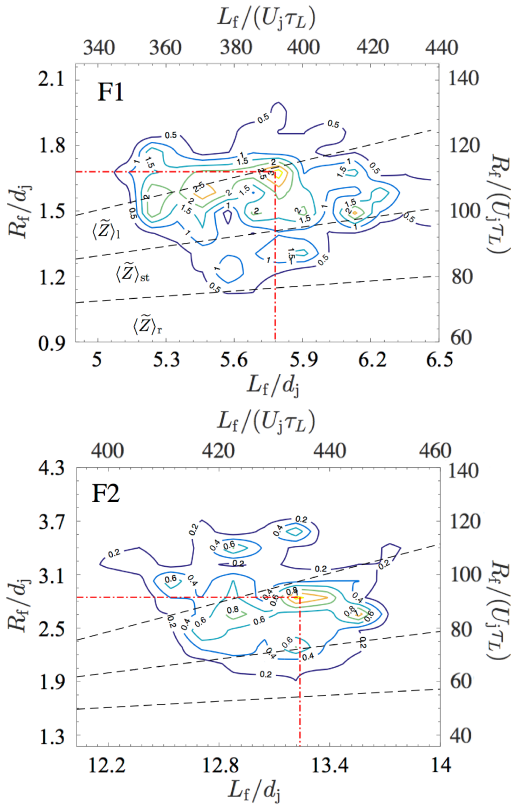

Fig. 7. Joint PDF of the stabilisation axial and radial locations. $\langle\widetilde{Z}\rangle_{st}$, $\langle\widetilde{Z}\rangle_l$ and $\langle\widetilde{Z}\rangle_r$ correspond to stoichiometry, lean and rich flammability limits respectively.

between F1 and F2 for the scaling using $U_j\tau_L$ suggesting a possibly strong correlation with the jet exit velocity. Also, the most probable locations are observed to be on the lean side of stoichiometry, very close to the lean flammability limit for both flames. However, it is less probable for the stabilisation point to appear on rich side because of high local flow velocity, which is similar to previous study on lifted jet flame in vitiated coflows [29]. To further explore this correlation between the radial location and mixture fraction, Fig. 8 shows the joint PDF of R_f and $\widetilde{Z}$ for both flames F1 and F2. It is clear that both flames are mostly stabilised

in the lean mixtures ($\widetilde{Z}_{\rm l} < \widetilde{Z} < \widetilde{Z}_{\rm st}$), having the most probable location at about $\widetilde{Z} = 0.08$ for F1 and $\widetilde{Z} = 0.06$ for F2. However, no evident correlation is observed between $R_{\rm f}$ and $\widetilde{Z}$ fluctuations suggesting that the radial stabilisation location may also depend on other physical processes such as large-scale flow structure and flame/turbulence interaction.

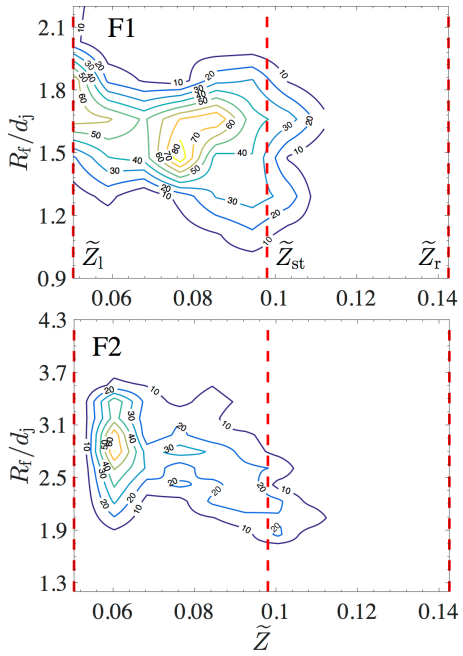

Fig. 8. Joint PDF of the mixture fraction and radial stabilisation location.

5. Conclusions

Transient evolution of edge flame in a spark-ignited methane-air jet is investigated numerically using LES with a sub-grid model for partially premixed combustion. Full sequence of ignition kernel development is simulated for two jet velocities with the same ignition location. Good agreement is obtained between

the LES and experimental results. The PDF of flame stabilisation location shows that both the axial and radial location are correlated to the jet exit velocity. Visualisation of the flame leading point trajectory is *spiral*-like during the edge flame propagation stage, in which two sub-stages are identified showing different propagation behaviours. The flame/flow interaction becomes more significant after the leading edge is within approximately $5d_{\mathrm{j}}$ of the lift-off height and the propagation characteristics are balanced among many physical processes.

Acknowledgements

ZC acknowledges the financial support of Cambridge Overseas Trusts and China Scholarship Council. SR and NS acknowledge the support of European Union funding through the project AMEL. The support of EPSRC is acknowledged by NS. This work used the ARCHER UK National Supercomputing Service (http://www.archer.ac.uk).

References

[1] E. Mastorakos, Prog. Energy Combust. Sci. 35 (2009) 57–97.

[2] J. Buckmaster, Prog. Energy Combust. Sci. 28 (2002) 435–475.

[3] A.R. Masri, Proc. Combust. Inst. 35 (2015) 1115–1136.

[4] N. Peters, Turbulent Combustion, Cambridge University Press, 2000.

[5] W.M. Pitts, Proc. Combust. Inst. 22 (1988) 809–816.

[6] K.M. Lyons, Prog. Energy Combust. Sci. 33 (2007) 211–231.

[7] C.J. Lawn, Prog. Energy Combust. Sci. 35 (2009) 1–30.

[8] A.D. Birch, D.R. Brown, M.G. Dodson, Proc. Combust. Inst. 18 (1981) 1775–1780.

[9] M.T.E. Smith, A.D. Birch, D.R. Brown, M. Fairweather, Proc. Combust. Inst. 21 (1986) 1403–1408.

[10] S.F. Ahmed, E. Mastorakos, Combust. Flame 146 (2006) 215–231.

[11] S.R. Tieszen, D.W. Stamps, T.J. O'Hern, Combust. Flame 106 (1996) 442–466.

[12] C.M. Müller, H. Breitbach, N. Peters, Proc. Combust. Inst. 25 (1994) 1099–1106.

[13] Z. Chen, S. Ruan, N. Swaminathan, Combust. Flame 162 (2015) 703–716.

[14] H. Pitsch, Annu. Rev. Fluid Mech. 38 (2006) 453–482.

[15] J. Janicka, A. Sadiki, Proc. Combust. Inst. 30 (2005) 537–547.

[16] M. Boileau, G. Staffelbach, B. Cuenot, T. Poinsot, C. Berat, Combust. Flame 154 (2008) 2–22.

[17] G. Lacaze, B. Cuenot, T. Poinsot, M. Oschwald, Combust. Flame 156 (2009) 1166–1180.

[18] V. Subramanian, P. Domingo, L. Vervisch, Combust. Flame 157 (2010) 579–601.

[19] G. Lacaze, E. Richardson, T. Poinsot, Combust. Flame 156 (2009) 1993–2009.

[20] W.P. Jones, V.N. Prasad, Proc. Combust. Inst. 33 (2011) 1355–1363.

[21] J. Smagorinsky, Mon. Weather Rev. 91 (1963) 99–164.

[22] S.B. Pope, Turbulent Flows, Cambridge University Press, 2000.

[23] S. Ruan, N. Swaminathan, O.R. Darbyshire, Combust. Theory Model. 18 (2014) 295–329.

[24] R.W. Bilger, S.H. Stårner, R.J. Kee, Combust. Flame 80 (1990) 135–149.

[25] H. Pitsch, H. Steiner, Phys. Fluids 12 (2000) 2541.

[26] N. Swaminathan, K.N.C. Bray, Combust. Flame 143 (2005) 549–565.

[27] T.D. Dunstan, Y. Minamoto, N. Chakraborty, N. Swaminathan, Proc. Combust. Inst. 34 (2013) 1193–1201.

[28] I. Langella, N. Swaminathan, Y. Gao, N. Chakraborty, Combust. Theory Model. 19 (2015) 628–656.

[29] M. Ihme, Y.C. See, Combust. Flame 157 (2010) 1850–1862.

List of Figures